Understanding the Mechanisms of Gold Shell Growth onto Polymer Microcapsules to Control Shell Thickness

Alison Tasker[1,2]*, James Hitchcock[1], Elaine A. Baxter[1], Olivier J. Cayre[1] and Simon Biggs[3]

[1]School of Chemical and Process Engineering, University of Leeds, Woodhouse Lane, Leeds, LS2 9JT.

[2]School of Chemical Engineering, University of Queensland, St Lucia, Queensland 4072

[3]Faculty of Engineering, Architecture and Information Technology, University of Queensland, St Lucia, Queensland 4072

Email: a.tasker@uq.edu.au

Abstract

Polymer microcapsules have been used commercially for decades, however they have an inherent flaw which renders them impractical as a carrier of small, volatile molecules. The porous nature of the polymer shell allows for diffusion of the encapsulated molecules into the bulk. The use of metal shells is an innovative way to prevent undesired loss of small molecules from the core of microcapsules, however it is important, particularly when using expensive metals to ensure that the resulting shell is as thin as possible.

Here we investigate the fundamental mechanisms controlling the gold shell thickness when a fragrance oil is encapsulated in a poly(methyl methacrylate) shell. We consider the distribution of the nanoparticles on the capsule surface, and from quantification of the adsorbed NP density and resulting shell thickness, we propose mechanisms to describe the gold shell growth for systems with high and low NP surface coverage. We suggest from our observations that the gold grows to fill in the gaps between NPs. At low NP concentrations, thicker metal shells form. We postulate that this is due to the low NP density on the surface, forcing the gold clusters to grow larger before they meet the adjacent ones. Thus, to grow the thinnest possible shells a densely packed monolayer of platinum nanoparticles is required on the capsule surface.

Introduction

Microencapsulation is a frequently used approach to control the delivery of active molecules and is used in a number of industries including agrochemicals,[1] pharmaceuticals,[2, 3] home and personal care,[4] paints,[5] and foods.[6] Most of the microcapsules used in industrial applications

today are traditional polymer-shell systems but although they are generally simple to manufacture, such microcapsule systems possess severe limitations for the retention and thus the delivery of small actives. Indeed, polymer-based microcapsule membranes are highly permeable to low molecular weight active compounds.[7] Several methods have been suggested for reducing the leakage rate of such small molecules from microcapsules.[8-10] For example Dowding et al. investigated the effect of increasing the thickness of the polymer shell to inhibit release, and also cross-linking the polymer to reduce its porosity.[8] Whilst they did see an improvement in core retention, they were unable to completely prevent losses from the core. Antipov et al. synthesised microcapsules using a layer-by-layer approach and found that by increasing the number of polyelectrolyte layers they could improve the core retention time, but only by minutes.[9] In addition, Zieringer et al. have shown that microfluidic methods can be used to form polymer microcapsules with a fluorinated shell, which was shown to retain 98% of dissociated $CaCl_2$ ions over a period of four weeks in an aqueous continuous phase.[11] These authors also demonstrated that by manipulating the osmotic pressure difference between the interior and exterior of the microcapsules, release of the salt could be triggered. However, when using organic solvents as the continuous phase, the release of the encapsulated small actives was more rapid. Despite its drastically improved core retention, this method still suffers from the fact that production of microcapsules through microfluidic channels is not yet a scalable technology. In an earlier publication, we reported an alternative approach for the manufacture of impermeable metal coated microcapsules using an electroless plating technique.[7] In this previous work, we demonstrated the ability of such metal-coated microcapsules to fully retain a small, volatile molecules on timescales of the order of months in an environment that fully dissolves these molecules. We also demonstrated the drastic influence of the catalytic nanoparticle surface density on the quality of the deposited second metal layer. This is particularly important as small defects in the microcapsule metal coating induces rapid release of the core when in contact with a solubilising bulk phase, while a continuous metal shell provides impermeability. Therefore, this current work aims to explore several parameters leading to differences in the nanoparticle surface density and to contribute to an improved understanding of the growth mechanism of the second metal film through electroless plating.

Electroless plating is a process by which a metal is reduced onto a surface from its salt initially dissolved in the bulk, without the need for an applied electrical potential.[12] Metal nanoparticles of either the same metal or a complementary metal are often used as a catalyst

for the plating reaction, and can be used to spatially locate the deposition of the plated metal on the surface of interest.[13-18] There are a great many applications reported for electroless deposition, particularly in electronic materials fabrication, such as for circuit boards,[19] conductors,[20] optical devices,[21] and electromagnetic shielding.[22]

A number of electroless deposition studies have been conducted on 3-dimensional surfaces, such as polymer beads,[23-25] and more recently microcapsules.[7, 26] Our approach involves first the preparation of a polymeric core-shell microcapsule from an oil-in-water emulsion,[7] using the method of Loxley and Vincent,[27, 28] then adsorbing poly(vinyl pyrollidone) (PVP)-stabilised platinum nanoparticles to the polymer surface,[17] before using the catalytic properties of these nanoparticles to deposit a continuous metal layer around the microcapsules.[29]

A significant concern with this method is the associated cost of producing precious metal-coated capsules, as this will restrict the range of possible applications for the technology. While it is clear that the use of more affordable catalyst nanoparticle/second metal combination (to grow silver, copper or zinc films for example) can drastically reduce cost, the use of Pt nanoparticle catalysts for the growth of a gold shell has certain advantages, including the accepted use of gold surfaces in biological applications and not least the high reaction rate, yield and specificity of this metal combination. It is therefore interesting to use this particular electroless deposition reaction as an model system to explore our ability to understand and control the metal layer growth in this process.

In our previous work we demonstrated that it was possible to fully retain hexyl salicylate within polymeric capsules coated with a continuous ~ 70 nm gold shell. By reducing the metal shell thickness whilst maintaining a continuous impermeable shell, one can also drastically reduce production costs.

In order to achieve, thinner metal films via electroless deposition, the majority of the reported work uses plating time as the main control parameter.[24, 25, 30-33] However, Hrapovic et al. suggest that holes within otherwise continuous gold shells grown on a monolayer of gold nanoparticles are due to the large initial inter-particle spacing, preventing the gold nanoparticles from coalescing.[31] Choe et al. used a complexing agent which was added to the plating solution to control the final morphology of their silver shells, grown on a Fe@TiO_2 core-shell particle template.[25] They found that addition of a low concentration of tri-sodium

citrate encouraged the growth of two different morphologies of silver islands, larger, non-spherical ones and much smaller spheres. They postulated that the smaller nanoparticles were able to fill the gaps left by the larger islands, resulting in a continuous shell being formed. In our previous work we showed that it was possible to produce impermeable metal microcapsules, with control of the metal shell thickness using temperature as a variable to control the reaction rate.[7]

Our aim in this work is to further explore the influence of the catalytic nanoparticle layer and to understand the mechanism underpinning metal shell growth. In particular, we are interested in describing the role of the catalytic nanoparticle distribution on the capsule surface in determining the resulting film thickness. Finally, this work alongside others should allow for as thin a shell as possible to be achieved, improving cost efficiency without reducing performance.

Materials and Methods

a. Materials

Poly(methyl methacrylate) (PMMA) (120 kDa), cetyltrimethylammonium bromide (CTAB) 98%, dichloromethane (DCM) >99%, poly(vinyl pyrrolidone) (PVP) (40 kDa), chloroplatinic acid (H_2PtCl_6) 99%, chloroauric acid ($HAuCl_4$) 99.99%, 30% hydrogen peroxide, hexyl salicylate 99%, and sodium borohydride, 98%, were obtained from Sigma-Aldrich and used as received. All solutions were prepared using ultrapure Milli-Q water (resistivity of ~18 $M\Omega.cm^{-1}$).

b. Preparation of gold coated PMMA microcapsules with a hexyl salicylate core

The method used was adapted from the previous work of Hitchcock et al.[7] PMMA (10g) was dissolved in DCM (76g) before hexyl salicylate (14g) was added and mixed until a single phase was formed. In the case of PMMA sphere synthesis the hexyl salicylate was not added. CTAB (0.28g) was dissolved into 100 mL Milli-Q water to form the continuous phase. The polymer phase (7 mL) and continuous phase (7 mL) were added to a glass vial and emulsified (IKA T25 Ultra-Turrax) at 15 000 rpm for 2 min. The resulting emulsion was then stirred magnetically at 400 rpm while a further 86 mL of continuous phase was added over 60 seconds. The diluted emulsion was then stirred at 400 rpm for 24 h at room temperature. The resulting PMMA core-shell microcapsules underwent three washing steps via

centrifugation/re-dispersion (Heraeus Megafuge R16 at 4000 rpm for 5 min). Each time, the supernatant was removed and replaced with fresh Milli-Q water. Finally, the capsules were redispersed in 50 mL Milli-Q water.

The PMMA capsules (1.0 mL, 2 wt %) were then added to a pre-prepared PVP stabilised Pt nanoparticle suspension (10 mL), as described in Hitchcock et al,[7] and mixed for 30 min at 30 rpm. The PVP-Pt solution was diluted to 70%, 50%, 30%, 25%, 12.5% and 2% of original concentration to study the effect of nanoparticle concentration on the adsorption density and the resulting secondary metal shell thickness. The PVP-Pt loaded capsules were immediately washed three times by centrifugation/re-dispersion at 4000 rpm for 5 min. Each time, the supernatant was removed and replaced with fresh Milli-Q water. The capsules were subsequently redispersed in 30 mL Milli-Q water.

The adsorption time was varied for the 50% diluted nanoparticle sample between 1 min and 4 h to investigate its effect on the resulting secondary metal shell thickness.

$HAuCl_4$ (1 mL, 40 mM), hydrogen peroxide (1 mL, 60 mM) and poly(vinyl pyrollidone) (1 mL, 0.05 mM) constituted the electroless plating solution. The PVP-Pt loaded polymer capsules (3 mL, 0.6 wt %) were added dropwise to the plating solution and stirred vigorously for 5 min. The metal-coated capsules were subsequently washed by centrifugation at 4000 rpm for 5 min, three times.

c. Analysis of metal shell and nanoparticle layer thickness

To analyse the thickness of adsorbed nanoparticle layers and the subsequent metal shell thickness, capsule samples were, after careful cleaning, set in an epoxy resin and 60 nm microtome slices of each sample were obtained. These samples were then examined by Transmission Electron Microscopy (TEM) (JEOL 1010) and analysed using ImageJ (imagej.net) image processing software.[34]

Under the TEM, the contrast between the metal and the polymer in the shell is very clear. This allows for simple measurements of thickness of the metal shell, as well as observations of spatial variation in the film properties. However, it is important to realise that each capsule cross section may not necessarily be taken across the centre of the capsule sphere. The point at which the image of the shell is expected to be thinnest (the actual shell thickness) will be at the equator of the capsule, and as we move further away from that point the metal shell will appear thicker, for example, at the top or bottom of the capsule, a 60 nm slice may result in a complete gold circle, with no polymer present. This, of course, is not representative of the

actual shell thickness, and to account for this, cross section images of many capsules must be analysed and plotted as a frequency distribution to find the most frequent length, which will correspond to the minimum shell thickness. Further complications are found in the uneven nature of the surface of the metal shells. This must also be taken into consideration to minimise errors in the determined shell thicknesses.

If we initially consider a model sample of perfectly smooth and spherical microcapsules, and assume a uniform size distribution, we can generate an expected frequency distribution as demonstrated in figure 1. By comparing this size distribution to the experimental data determined from a sample of capsules with an uneven surface and of non-uniform size, we observe that these two parameters effectively extend the curve laterally; but, we obtain the same maximum peak as seen for the theoretical data. This confirms that the most frequent length corresponds to the actual shell thickness, regardless of the surface morphology, if we analyse sufficiently large numbers of capsules.

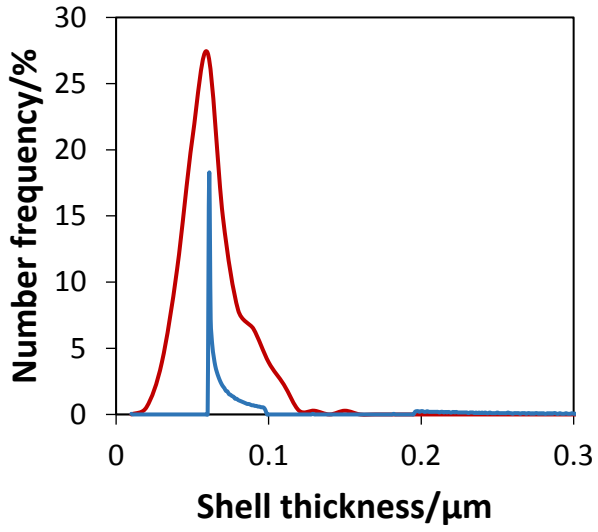

Figure 1 - Theoretical frequency plot for smooth, uniform 2 µm capsules with a metal shell of 60 nm (blue) vs frequency (number of incidents of a particular shell thickness) plot of data measured from experimental capsule sample with $6.3x10^4$ PVP-Pt np's added per capsule surface area (μm^2) (red).

d. Nanoparticle adsorption using UV spectrophotometry

UV absorbance spectra were measured using an Agilent Cary 4000 UV-vis spectrophotometer to assess the nanoparticle adsorption onto a known surface area of polymer capsules. The capsule supernatant was analysed after washing. The baseline was established against a sample blank of 0.0625 wt% PVP in order to prevent interference in the

region of interest in the spectra. For adsorption times of 2 minutes or less the supernatant was diluted 10 times using Milli-Q water before absorbance was measured. The measured nanoparticle concentration in the supernatant was subtracted from the initial nanoparticle concentration added to the microcapsules to determine the adsorbed nanoparticle number on the microcapsules. A calibration curve of nanoparticle concentration versus absorbance was initially established to allow the concentration of nanoparticles remaining in the supernatant to be easily determined (Fig. S2 in supplementary information).

e. Characterisation

Size distribution of polymer microcapsules was conducted on a Malvern Mastersizer (Malvern Instruments, Asia Pacific). Capsule morphology of the NP-adsorbed capsules was conducted on a JEOL 1010 transmission electron microscope (JEOL, USA). Scanning electron microscopy was used to investigate polymer and gold shell capsule morphologies, using a Hitachi SE3500 scanning electron microscope (Hitachi, Asia Pacific). Chemical composition of the microcapsules was analysed using an Oxford Instruments energy dispersive x-ray spectrometer attached to a JEOL 7001 field emission SEM (JEOL, USA).

Results and Discussion

The aim of this work is to ascertain how nanoparticle adsorption onto the polymer microcapsule surface affects the resulting metal shell growth and final thickness. The polymer microcapsules were prepared as described in our previous work using a solvent evaporation method[7] with hexyl salicylate, a commonly used fragrance oil, as the core material. In accordance with our previous findings, core-shell microcapsules with an average size of 10 μm were obtained. Platinum nanoparticles, stabilised with poly(vinyl pyrrolidone) were physically adsorbed to the surface of the polymer microcapsules, and the NP concentration and adsorption time were varied to aim for varied NP adsorbed densities. Gold films were deposited onto PMMA capsules by electroless deposition using the platinum nanoparticles initially physisorbed onto the shells as a catalyst (SEM images of the gold shells produced under various conditions can be found in figure S1 of the supplementary information).

Gold-coated capsules, from each of the samples, were set in an epoxy resin and microtome slices were taken at 60 nm intervals to enable observation of a large population of capsule cross-sections. Under the TEM, the gold shells are seen as dark rings contrasting with the lighter polymer and resin. As a result the microcapsule metal shell thickness can easily be measured using the image analysis software, imageJ, as described in the methods section. The maxima of the frequency plots generated from analysis of the measured shell thicknesses was used to obtain the reported average measurement of the sample shell thickness from the cross-sections. It is important to note here that the diamond knife used to slice the capsules embedded in resin can cause the capsules to deform in the direction of the cutting action (so they appear more oval instead of spherical) and because of this it can also cause imperfections to appear in the shell.

Metal shell thickness was measured following the procedure described above for microcapsules exposed to different initial concentrations of nanoparticles as shown in Figure 2. As the number of nanoparticles added to the polymer microcapsule suspension is increased, for a fixed surface area of capsules and at a fixed adsorption time, a clear reduction in the thickness of the resultant secondary metal film produced through the electroless deposition process is initially observed, until a plateau is reached at $> 6 \times 10^4$ nanoparticles per μm^2 of capsule surface area. An initial hypothesis based on these data suggests that nanoparticle arrangements in the adsorbed film directly impacts the thickness of the final metal shell, supported by the data shown in figure 4, which will be discussed in more detail

later in the article, which shows that the adsorbed density of nanoparticles increases with increasing nanoparticle concentration used, at least until a concentration of 6.3 x 10^4 nanoparticles per μm^2 of capsule surface area.

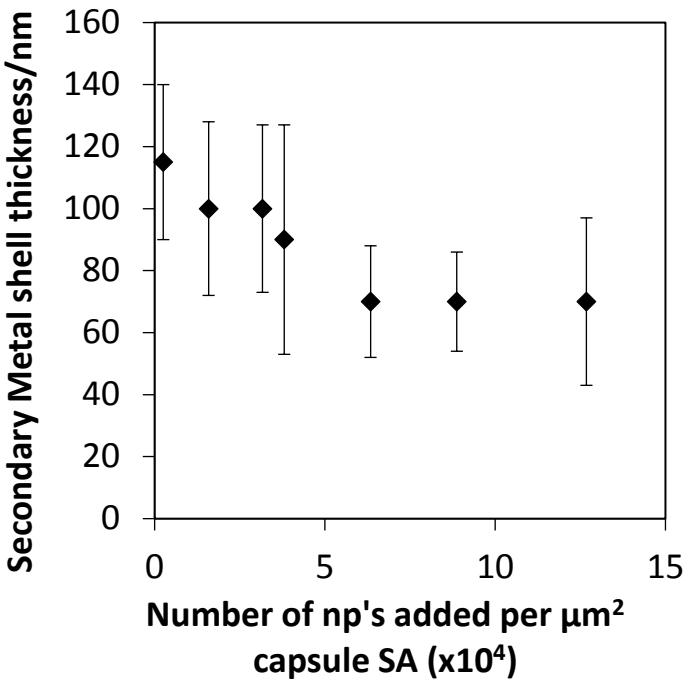

Figure 2 - Microcapsule secondary metal shell thickness as a function of increasing concentration of nanoparticles during the initial nanoparticle catalysts adsorption stage. In all experiments, microcapsule surface area is maintained constant alongside adsorption time (30 minutes at ambient temperature).

Based on our previous findings, the adsorption density of PVP-Pt nanoparticles onto PMMA capsules with a different oil core (toluene) was controlled by changing the concentration of the nanoparticle dispersions, with a maximum coverage by the metal NP core ~5% of the surface (with the remainder of the NP occupied area covered by the PVP polymer stabiliser), representing a hexagonally close packed monolayer.[7] Thus, if we consider the adsorbed nanoparticle layer to be a monolayer, then a possible explanation for the difference in shell thickness at low and high coverage of nanoparticles on the polymer surface is given in the schematic shown below (figure 5). Horiuchi et al. describe how platinum nanoparticles can spatially locate and direct the growth of gold films.[17] They show that when gold deposits are selectively removed from a 2D film of polymer embedded with PVP-Pt that had previously been subjected to electroless gold deposition, Pt NPs are clearly visible via TEM, where the gold deposits once were. As a result, we may expect the gold film to initially nucleate and

grow from the adsorbed platinum nanoparticles (in this case acting as seeds) during the electroless plating process. As the added nanoparticle concentration increases, the density of the nanoparticles adsorbed on the polymer surface will increase, leading to a reduction in inter-particle spacing. Thus, we may expect that for adjacent nanoparticle centres with larger inter-particle spacing to fuse together, proportionately larger amounts of gold will be required to deposit and grow (Figure 3a) to form a complete shell, than for the case where the nanoparticles are closer together (Figure 3b). This suggests that in order to get the thinnest possible gold films, a higher density of efficiently packed (e.g. a 2D hexagonal array) nanoparticles is preferred so that a minimum amount of precipitating gold is required to fill in the inter-nanoparticle gaps.

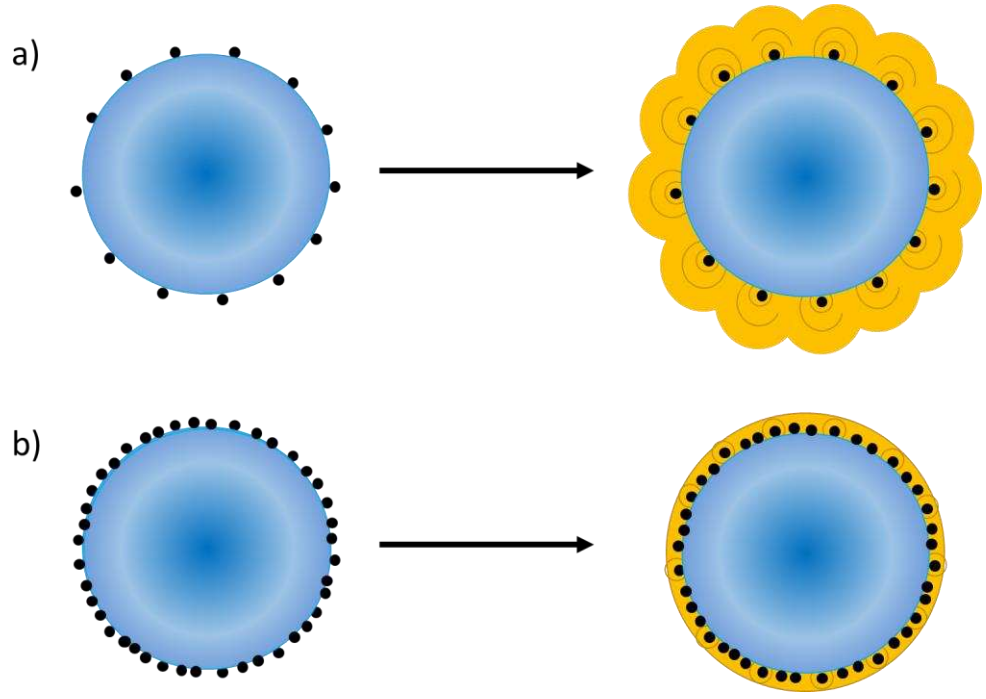

Figure 3 - Schematic diagrams of proposed mechanism of gold growth onto a single layer nanoparticle film when a) low density and b) high density of nanoparticles are adsorbed to the polymer surface.

UV-vis spectroscopy was conducted on the supernatant once the nanoparticle adsorption process onto the capsules was complete. By deducing the number of nanoparticles remaining in the bulk from these measurements, the number of adsorbed nanoparticles on the microcapsule surface was calculated. We found that after 30 minutes, there were few nanoparticles remaining in the bulk and essentially all the nanoparticles that were added were adsorbed to the capsules at the three concentrations tested here (fig 4). These concentrations were all well above that required for a simple monolayer, indicating a likelihood of multiple layers of nanoparticles forming on the capsules.

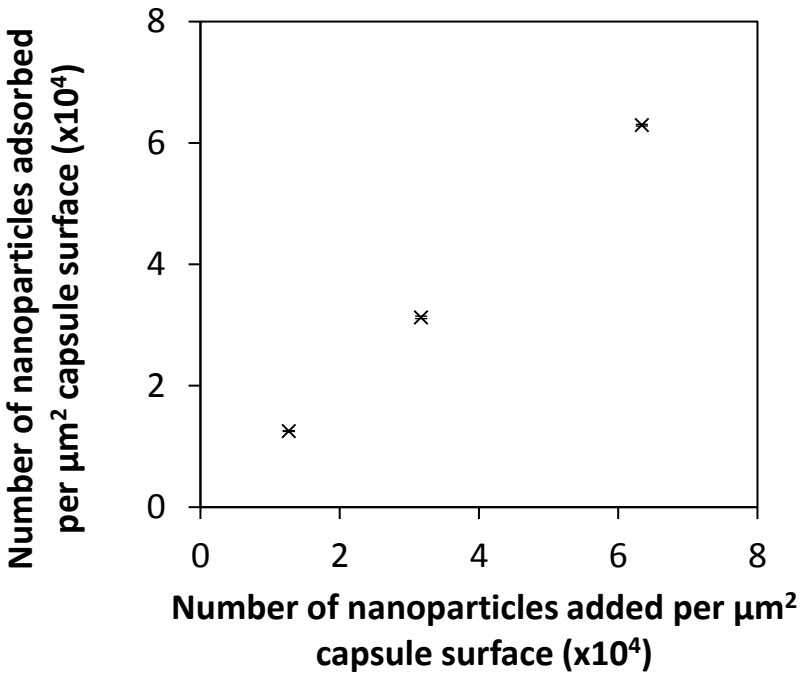

Figure 4 - Number of nanoparticles adsorbed to polymer microcapsule surface as a function of the number initially added to the polymer microcapsule sample. Experiments were conducted at room temperature with an adsorption time of 30 min.

To further explore the proposed mechanism of gold film growth, the time allowed for nanoparticle adsorption was varied for the case where 6.3×10^4 nanoparticles were added per μm^2 of capsule surface. This sample was chosen because the nanoparticle concentration used in this case was the lowest for the thinnest gold shells obtained. Figure 5 shows that there is no discernible increase in gold metal shell thickness with NP adsorption time, except for small differences at very low adsorption times. This suggests that the nanoparticle adsorption occurs rapidly since little or no reduction in film thickness is observed even for short adsorption times. No significant effect of NP adsorption time was also observed at a different concentration of 1.6×10^4 nanoparticles per μm^2 of capsule surface.

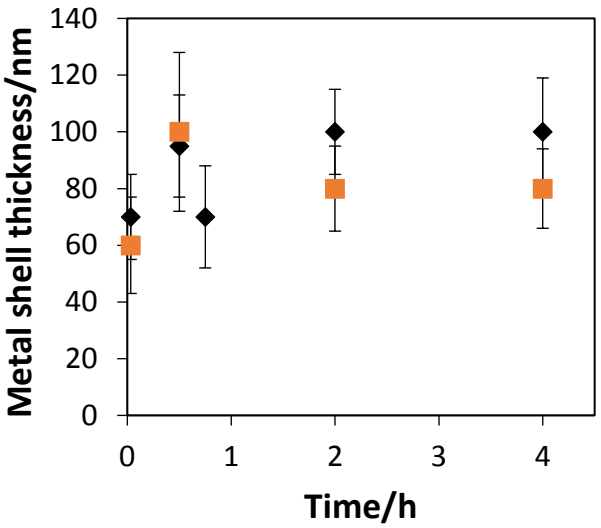

Figure 5 - Metal shell thickness as a function of nanoparticle adsorption time for $6.3x10^4$ nanoparticles per μm^2 of capsule surface area (black) and $3.2x10^4$ nanoparticles per μm^2 of capsule surface area (orange). Adsorption occurred at ambient temperature.

By measuring light absorbance of the capsule suspension supernatant after nanoparticle adsorption using UV spectrophotometry, the concentration and thus the number of nanoparticles remaining in the supernatant was estimated (against a calibration curve obtained under the same conditions see Figure S2). On the basis of these data, the number of nanoparticles adsorbed to the capsule surface was indirectly obtained via mass balance between the initial concentration of nanoparticles in the suspension and the concentration remaining in the supernatant following the adsorption process. From this an equivalent number of particle monolayers (assuming hexagonal packing of the NP on the microcapsule surface) was calculated and these data are presented in Figure 6. These results suggest that the PVP-Pt nanoparticles are either forming multi-layers on the microcapsule surface or are adsorbing as aggregated species. It should be noted that hexyl salicylate has low solubility in water (0.009 mg/mL), and so a small volume of the oil can diffuse out of the polymer shell. To deduce whether the adsorption conditions caused NP aggregation, a small volume of hexyl salicylate was added to the NP dispersion, causing immediate destabilisation of the dispersion. These data also confirm that the adsorption process is rapid with significant coverage seen after just 2 min. The number of nanoparticles adsorbed is relative to the initial concentration added to the microcapsule suspension, and in these cases more than 95% of the available nanoparticles have been adsorbed (fig 4), suggesting that the range of NP concentrations investigated here reside within the linear region of the adsorption isotherm.

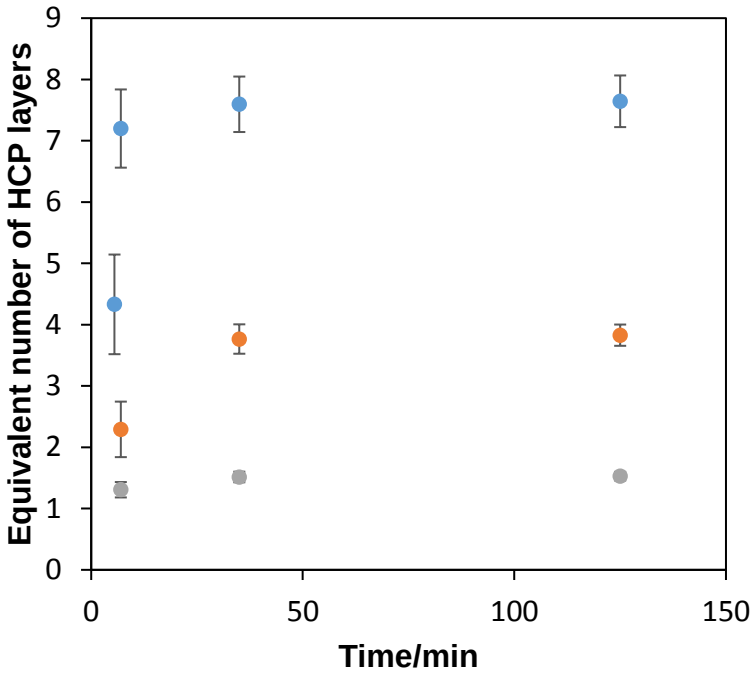

Figure 6 - Resulting equivalent number of hexagonally close packed 2D layers on capsule surface with adsorption time calculated from UV absorbance of nanoparticles remaining in supernatant after adsorption and washing stages at ambient temperature. $6.3x10^4$ nanoparticles (blue), $3.2x10^4$ nanoparticles (orange), $1.3x10^4$ nanoparticles (grey) per μm^2 capsule surface area.

To further understand how the nanoparticles adsorb to the microcapsules, microtome slices of the nanoparticle-loaded capsules (i.e. prior to electroless plating) embedded in resin were taken and viewed under TEM. Representative examples of the micrographs obtained are shown in figure 7.

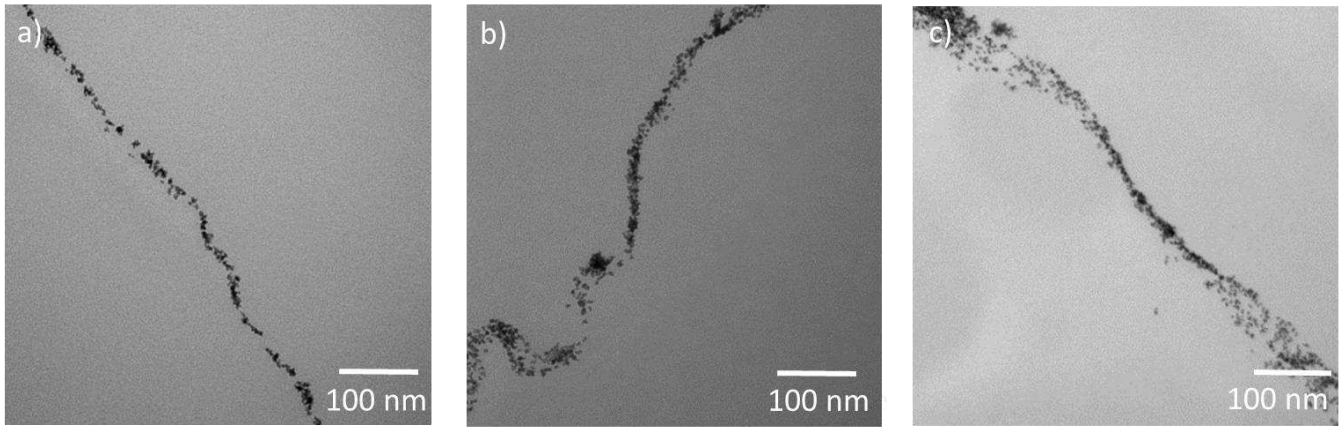

Figure 7 - Transmission electron micrographs showing cross sections of polymer capsules with nanoparticles adsorbed from various concentrations, a) $1.3x10^4$ b) $3.2x10^4$ and c) $6.3x10^4$ nanoparticles per μm^2 capsule surface area, adsorbed for 30 minutes.

These micrographs show that as more nanoparticles are added, an aggregated layer, which forms on the capsule surface, becomes thicker and covers progressively more of the surface. The distribution of nanoparticles on the capsule surface is uneven, with clusters of aggregated nanoparticles in some parts, along with thinner, more densely packed layers in others. When a lower concentration of nanoparticles is added, large gaps in the nanoparticle coverage can be seen (figure 7a), but even at this concentration multiple (incomplete) layers are formed, confirming the data (grey data points) presented in figure 6, where we observe the equivalent of approximately 1.5 monolayers of nanoparticles adsorbed to the capsules, for an adsorption time of 30 minutes. Figure 7b and c suggests an open and relatively porous film of nanoparticles is formed on the polymer shell, with many more layers adsorbed as the nanoparticle concentration is increased.

At this stage of the investigation, the schematic presented in Figure 2 therefore needs to be revisited as it appears to represent a somewhat simplistic representation of the observed system behaviour. An alternative mechanism of gold film growth is therefore suggested where the gold must penetrate into the porous adsorbed nanoparticle layer and grow to fill in the pores, thereby forming a complete layer. The presence of a fractal nanoparticle layer in this particular system may explain why the gold shell thickness remains at 70 nm, as there are parts of the nanoparticle layer which stretch to this distance from the polymer surface. The nanoparticle coverage seen in figure 7 is not uniform over the whole capsule surface, likely due to the marginal stability of the nanoparticles and associated aggregation leading to both aggregate and single particle adsorption. The nanoparticle instability seen on the capsule surface is also likely to be due to the interaction between the core material and nanoparticle polymer stabiliser, which is perhaps plasticised by the hexyl salicylate core oil. Indeed, when a small volume of hexyl salicylate is added to the nanoparticle suspension (i.e. saturating the aqueous phase with the oil), nanoparticle destabilisation occurs, which was verified by visual observation as the nanoparticles aggregated and precipitated to leave a colourless aqueous phase (figure S3 in supplementary information). This marginal stability is somewhat desirable in that it likely improves the nanoparticle affinity for the polymer surface. In our previous work where toluene was used as the core material, nanoparticle aggregation is not induced by the presence of the oil, suggesting that the polymer microcapsule chosen core oil plays a significant role in the adsorption of the nanoparticles (see figure S4 in supplementary

information). Using $1.3x10^4$ nanoparticles per μm^2 of spheres, with a 30 minute adsorption time it is clear from transmission electron micrographs that non-uniform multilayers occur on the hexyl salicylate core capsules (fig S4 in supplementary information). Based on the nanoparticle distributions observed using TEM, figure 8 illustrates possible alternative mechanisms of growth at different surface coverages of aggregated nanoparticles as a schematic.

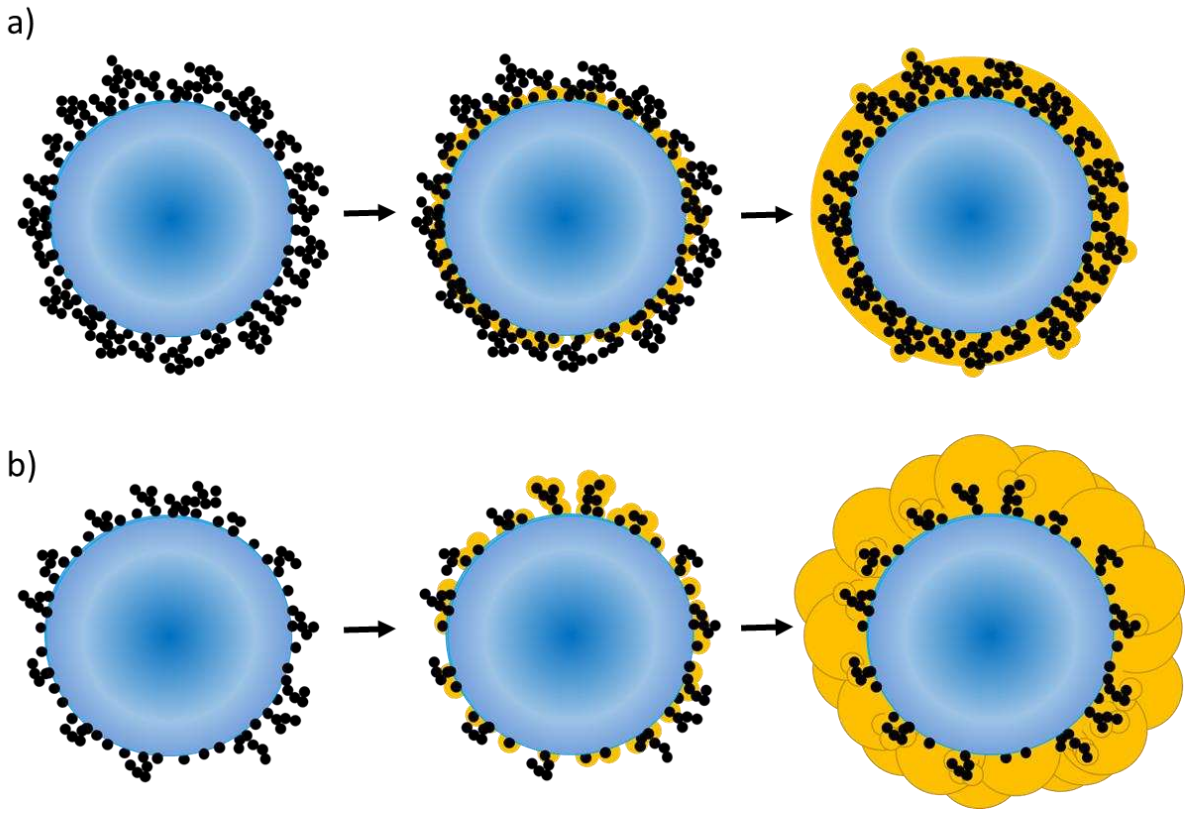

Figure 8 - Schematic diagram of proposed mechanisms of gold growth when a) a dense but porous network of nanoparticles cover the surface to form non-homogenous multi-layers, and b) nanoparticles form clusters which sporadically adsorb to the capsule surface resulting in low density coverage.

It is anticipated that at a low density of nanoparticle clusters, initially the gold would fill in the open structure formed by the clusters, then continue to nucleate and grow until fusing with an adjacent cluster, similar to the mechanism presented in figure 3a, but with larger catalytic sites. As the nanoparticle clusters are unevenly distributed across the surface when a lower concentration of nanoparticles is added to the capsules (figure 7a), the gold clusters are likely to grow larger before fusing, resulting in the thicker films as seen in figure 3 for lower nanoparticle concentrations. Considering the nanoparticle structures seen in figure 7b and c

when higher nanoparticle concentrations are used, we expect that the gold will also penetrate the open structure formed by the nanoparticles, growing to fill in the gaps, without limited further growth required to form a complete shell. This theory is supported by the transmission electron micrographs of gold shells, shown in figure 9. These are representative microtome slices of the sample where $6.3x10^4$ nanoparticles per capsule surface (μm^2) were added (as seen prior to gold coating in figure 7c). The gold shell thickness shown here is seen to be of the same order of magnitude as the nanoparticle layer, around 70 nm, confirming that the gold most likely grows within, and fills, the porous film.

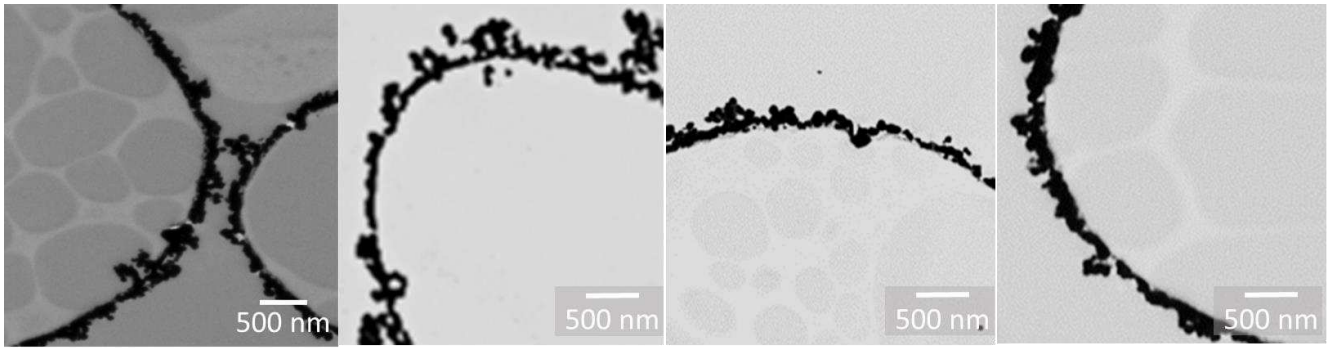

Figure 9 – Representative transmission electron micrographs showing cross sections of gold-coated polymer capsules with $6.3x10^4$ nanoparticles added per μm^2 capsule surface area.

Whilst the mechanism of metal shell growth is now somewhat clearer, a thinner shell has still not been achieved. In order to optimise the system, a highly packed monolayer of nanoparticles is still required to limit the ultimate thickness of the metal shell produced, following the mechanism suggested in figure 3b. Our future work will investigate how to better control the nanoparticle adsorption to achieve a single, close packed monolayer, in order to grow impermeable and more cost efficient gold shells on polymer microcapsules.

Conclusions

This work aimed to develop a fundamental understanding of the mechanism of metal shell growth on polymeric capsules with a view to optimising the capsules to be more cost efficient. We have found that for the manufacture of metal-coated microcapsules, the total nanoparticle loading, and associated spatial arrangement of these nanoparticles, onto the preformed polymer capsule surface is clearly important in determining the metal shell thickness when using electroless plating. Lower surface coverage is seen here to give thicker metal shells. The adsorption of nanoparticles onto the polymer capsule surface occurs very

rapidly, with more than the equivalent of a monolayer adsorbing in a few minutes. By exploring the nanoparticle distribution of the capsule surface, it has been shown that close packed monolayers were not formed, but that the nanoparticles were aggregating and formed multilayers on the microcapsule surface, likely as a result of destabilisation through interaction with the small amount of core oil dissolved in the continuous phase. Thus, we have proposed a mechanism, supported by quantification of the adsorbed nanoparticle density and by transmission electron microscopy observations of microcapsule cross-sections, to explain the growth of the metal shells whereby the metal penetrates through the porous nanoparticle network to complete the layer. The arrangement of the nanoparticle layer therefore determines the final metal shell thickness in the cases demonstrated in this study. Improving the stability of the nanoparticles may allow us to achieve a close packed monolayer of nanoparticles on which to grow the thinnest metal shells to optimise the system and improve cost efficiency.

1. Hedaoo, R. K.; Gite, V. V., Renewable Resource-Based Polymeric Microencapsulation of Natural Pesticide and Its Release Study: An Alternative Green Approach. Rsc Advances **2014,** 4 (36), 18637-18644.
2. Sun, C.; Shu, K.; Wang, W.; Ye, Z.; Liu, T.; Gao, Y.; Zheng, H.; He, G.; Yin, Y., Encapsulation and Controlled Release of Hydrophilic Pesticide in Shell Cross-Linked Nanocapsules Containing Aqueous Core. International Journal of Pharmaceutics **2014,** 463 (1), 108-114.
3. Pekarek, K. J.; Jacob, J. S.; Mathiowitz, E., Double-Walled Polymer Microspheres for Controlled Drug-Release. Nature **1994,** 367 (6460), 258-260.
4. Li, Y.; Huang, Y.-Q.; Fan, H.-F.; Xia, Q., Heat-Resistant Sustained-Release Fragrance Microcapsules. Journal of Applied Polymer Science **2014,** 131 (7).
5. Fay, F.; Linossier, I.; Legendre, G.; Vallee-Rehel, K., Micro-Encapsulation and Antifouling Coatings: Development of Poly(Lactic Acid) Microspheres Containing Bioactive Molecules. Macromol. Symp. **2008,** 272, 45-51.
6. Yang, Z.; Peng, Z.; Li, J.; Li, S.; Kong, L.; Li, P.; Wang, Q., Development and Evaluation of Novel Flavour Microcapsules Containing Vanilla Oil Using Complex Coacervation Approach. Food Chemistry **2014,** 145, 272-277.
7. Hitchcock, J. P.; Tasker, A. L.; Baxter, E. A.; Biggs, S.; Cayre, O. J., Long-Term Retention of Small, Volatile Molecular Species within Metallic Microcapsules. Acs Applied Materials & Interfaces **2015,** 7 (27), 14808-14815.
8. Dowding, P. J.; Atkin, R.; Vincent, B.; Bouillot, P., Oil Core/Polymer Shell Microcapsules by Internal Phase Separation from Emulsion Droplets. Ii: Controlling the Release Profile of Active Molecules. Langmuir **2005,** 21 (12), 5278-5284.
9. Antipov, A. A.; Sukhorukov, G. B.; Donath, E.; Möhwald, H., Sustained Release Properties of Polyelectrolyte Multilayer Capsules. The Journal of Physical Chemistry B **2001,** 105 (12), 2281-2284.

10. Lee, H.; Choi, C.-H.; Abbaspourrad, A.; Wesner, C.; Caggioni, M.; Zhu, T.; Weitz, D. A., Encapsulation and Enhanced Retention of Fragrance in Polymer Microcapsules. ACS Applied Materials & Interfaces **2016**.
11. Zieringer, M. A.; Carroll, N. J.; Abbaspourrad, A.; Koehler, S. A.; Weitz, D. A., Microcapsules for Enhanced Cargo Retention and Diversity. Small **2015,** 11 (24), 2903-2909.
12. Mallory, G. O.; Hajdu, J. B.; Electroplaters, A.; Society, S. F., Electroless Plating: Fundamentals and Applications. The Society: 1990.
13. Schaefers, S.; Rast, L.; Stanishevsky, A., Electroless Silver Plating on Spin-Coated Silver Nanoparticle Seed Layers. Materials Letters **2006,** 60 (5), 706-709.
14. Tong, H.; Zhu, L.; Li, M.; Wang, C., Electroless Silver Deposition on Si(100) Substrate Based on the Seed Layer of Silver Itself. Electrochimica Acta **2003,** 48 (17), 2473-2477.
15. Inberg, A.; Livshits, P.; Zalevsky, Z.; Shacham-Diamand, Y., Electroless Deposition of Silver Thin Films on Gold Nanoparticles Catalyst for Micro and Nanoelectronics Applications. Microelectronic Engineering **2012,** 98, 570-573.
16. Byeon, J. H.; Kim, J.-W., Novel Electroless Copper Deposition on Carbon Fibers with Environmentally Friendly Processes. Journal of Colloid and Interface Science **2010,** 348 (2), 649-653.
17. Horiuchi, S.; Nakao, Y., Platinum Colloid Catalyzed Etchingless Gold Electroless Plating with Strong Adhesion to Polymers. Surface & Coatings Technology **2010,** 204 (23), 3811-3817.
18. Rohan, J. F.; O'Riordan, G.; Boardman, J., Selective Electroless Nickel Deposition on Copper as a Final Barrier/Bonding Layer Material for Microelectronics Applications. Applied Surface Science **2002,** 185 (3–4), 289-297.
19. Abbott, A. P.; Griffith, J.; Nandhra, S.; O'Connor, C.; Postlethwaite, S.; Ryder, K. S.; Smith, E. L., Sustained Electroless Deposition of Metallic Silver from a Choline Chloride-Based Ionic Liquid. Surface and Coatings Technology **2008,** 202 (10), 2033-2039.
20. Narkis, M.; Yacubowicz, J.; Vaxman, A.; Marmur, A., Electrically Conductive Composites Prepared from Polymer Particles Coated with Metals by Electroless Deposition. Polymer Engineering & Science **1986,** 26 (2), 139-143.
21. Coluccio, M. L.; Gentile, F.; Francardi, M.; Perozziello, G.; Malara, N.; Candeloro, P.; Di Fabrizio, E., Electroless Deposition and Nanolithography Can Control the Formation of Materials at the Nano-Scale for Plasmonic Applications. Sensors (Basel, Switzerland) **2014,** 14 (4), 6056-6083.
22. Huang, C.-Y.; Pai, J.-F., Optimum Conditions of Electroless Nickel Plating on Carbon Fibres for Emi Shielding Effectiveness of Encf/Abs Composites. European Polymer Journal **1998,** 34 (2), 261-267.
23. Siiman, O.; Burshteyn, A., Preparation, Microscopy, and Flow Cytometry with Excitation into Surface Plasmon Resonance Bands of Gold or Silver Nanoparticles on Aminodextran-Coated Polystyrene Beads. Journal of Physical Chemistry B **2000,** 104 (42), 9795-9810.
24. Lim, Y. T.; Park, O. O.; Jung, H.-T., Gold Nanolayer-Encapsulated Silica Particles Synthesized by Surface Seeding and Shell Growing Method: Near Infrared Responsive Materials. Journal of Colloid and Interface Science **2003,** 263 (2), 449-453.
25. Choe, W. G.; Kim, D. Y.; Park, O. O., Morphology Control and Temporal Growth of a Continuous Silver Shell on Core-Shell Spheres. Crystengcomm **2014,** 16 (23), 5142-5149.
26. Patchan, M. W.; Baird, L. M.; Rhim, Y.-R.; LaBarre, E. D.; Maisano, A. J.; Deacon, R. M.; Xia, Z.; Benkoski, J. J., Liquid-Filled Metal Microcapsules. ACS Applied Materials & Interfaces **2012,** 4 (5), 2406-2412.

27. Loxley, A.; Vincent, B., Preparation of Poly(Methylmethacrylate) Microcapsules with Liquid Cores. Journal of Colloid and Interface Science **1998,** 208 (1), 49-62.
28. Tasker, A. L.; Hitchcock, J. P.; He, L.; Baxter, E. A.; Biggs, S.; Cayre, O. J., The Effect of Surfactant Chain Length on the Morphology of Poly(Methyl Methacrylate) Microcapsules for Fragrance Oil Encapsulation. Journal of Colloid and Interface Science **2016,** 484, 10-16.
29. Njoki, P. N.; Jacob, A.; Khan, B.; Luo, J.; Zhong, C.-J., Formation of Gold Nanoparticles Catalyzed by Platinum Nanoparticles: Assessment of the Catalytic Mechanism. J. Phys. Chem. B **2006,** 110 (45), 22503-22509.
30. Liu, S.-f.; Li, J.-R.; Jiang, L., Surface Modification of Platinum Quartz Crystal Microbalance by Controlled Electroless Deposition of Gold Nanoparticles and Its Enhancing Effect on the Hs-DNA Immobilization. Colloids and Surfaces A: Physicochemical and Engineering Aspects **2005,** 257–258, 57-62.
31. Hrapovic, S.; Liu, Y. L.; Enright, G.; Bensebaa, F.; Luong, J. H. T., New Strategy for Preparing Thin Gold Films on Modified Glass Surfaces by Electroless Deposition. Langmuir **2003,** 19 (9), 3958-3965.
32. Kobayashi, Y.; Tadaki, Y.; Nagao, D.; Konno, M., Deposition of Gold Nanoparticles on Silica Spheres by Electroless Metal Plating Technique. Journal of Colloid and Interface Science **2005,** 283 (2), 601-604.
33. Chen, D.; Liu, H.-Y.; Liu, J.-S.; Ren, X.-L.; Meng, X.-W.; Wu, W.; Tang, F.-Q., A General Method for Synthesis Continuous Silver Nanoshells on Dielectric Colloids. Thin Solid Films **2008,** 516 (18), 6371-6376.
34. Schneider, C. A.; Rasband, W. S.; Eliceiri, K. W., Nih Image to Imagej: 25 Years of Image Analysis. Nat Meth **2012,** 9 (7), 671-675.